Brain Stimulation 17 (2024) 92–103

Contents lists available at ScienceDirect

Brain Stimulation

journal homepage: www.journals.elsevier.com/brain-stimulation

Pulse-width modulated temporal interference (PWM-TI) brain stimulation

Charlotte E. Luff [a,b], Patrycja Dzialecka [a,b], Emma Acerbo [c,e], Adam Williamson [c,d], Nir Grossman [a,b,*]

[a] Department of Brain Sciences, Imperial College London, London, United Kingdom
[b] UK Dementia Research Institute, Imperial College London, United Kingdom
[c] Institut de Neurosciences des Systèmes (INS), INSERM, UMR_1106, Aix-Marseille Université, Marseille, France
[d] International Clinical Research Center (ICRC), St. Anne's University Hospital, Brno, Czech Republic
[e] Department of Neurosurgery, Emory University, Atlanta, GA, USA

ARTICLE INFO

Keywords:
Non-invasive brain stimulation
Temporal interference
Deep brain stimulation

ABSTRACT

Background: Electrical stimulation involving temporal interference of two different kHz frequency sinusoidal electric fields (temporal interference (TI)) enables non-invasive deep brain stimulation, by creating an electric field that is amplitude modulated at the slow difference frequency (within the neural range), at the target brain region.

Objective: Here, we investigate temporal interference neural stimulation using square, rather than sinusoidal, electric fields that create an electric field that is pulse-width, but not amplitude, modulated at the difference frequency (pulse-width modulated temporal interference, (PWM-TI)).

Methods/Results: We show, using ex-vivo single-cell recordings and in-vivo calcium imaging, that PWM-TI effectively stimulates neural activity at the difference frequency at a similar efficiency to traditional TI. We then demonstrate, using computational modelling, that the PWM stimulation waveform induces amplitude-modulated membrane potential depolarization due to the membrane's intrinsic low-pass filtering property.

Conclusions: PWM-TI can effectively drive neural activity at the difference frequency. The PWM-TI mechanism involves converting an envelope amplitude-fixed PWM field to an amplitude-modulated membrane potential via the low-pass filtering of the passive neural membrane. Unveiling the biophysics underpinning the neural response to complex electric fields may facilitate the development of new brain stimulation strategies with improved precision and efficiency.

1. Introduction

Deep brain stimulation (DBS) via implanted electrodes has been used worldwide to treat patients with severe movement disorders, such as Parkinson's disease (PD) [1], and affective disorders, such as obsessive–compulsive disorder (OCD) [2]. In addition, DBS is being investigated as a treatment for other conditions, such as depression [3] and Alzheimer's disease (AD) [4,5]. However, the risk associated with inserting electrodes into the brain makes exploring different brain targets difficult, and limits potential therapeutic impact [1,6]. On the other hand, traditional non-invasive brain stimulation methods, such as transcranial alternating or direct current stimulation, have relatively poor focality and cannot stimulate deep brain structures at clinically applied current densities [7].

We recently discovered a strategy aimed at enabling non-invasive DBS, i.e., without brain surgery, by temporal interference (TI) of kHz electric fields [8]. We first validated the TI stimulation concept in rodents using phantom measurements, in-vivo single-cell electrophysiology and immunohistochemistry, showing non-invasive focal modulation of the mouse hippocampal activity [8]. We then validated the concept in humans using cadaver measurements, functional magnetic resonance imaging (fMRI) and behavioral tests, showing non-invasive focal modulation of the human hippocampal activity and augmentation of its memory function [9]. Since its original publication [8], TI brain stimulation has been used in numerous computational [10–14], and experimental studies in animal models [15–17] and humans [18,19] including non-invasive human DBS [9,20], and several clinical studies are ongoing worldwide (e.g. NIH: NCT05805215, NCT03747601, NCT04761471). It is important to note that current densities traditionally used in humans generate electric field magnitudes

* Corresponding author. Department of Brain Sciences, Imperial College London, London, United Kingdom.
E-mail address: nirg@imperial.ac.uk (N. Grossman).

https://doi.org/10.1016/j.brs.2023.12.010
Received 7 September 2023; Received in revised form 18 December 2023; Accepted 19 December 2023
Available online 23 December 2023
1935-861X/© 2024 The Authors. Published by Elsevier Inc. This is an open access article under the CC BY license (http://creativecommons.org/licenses/by/4.0/).

capable of subthreshold but not suprathreshold stimulation [7,9]. Like conventional transcranial alternating current stimulation (tACS), TI likely synchronizes neural spiking activity tuned to the endogenous oscillation frequency [21].

TI involves applying two sinusoidal electric fields $\overline{E}_1$ and $\overline{E}_2$ to the brain at slightly different kHz frequencies (f_1 and f_2) that are beyond the frequency range of normal neuronal activity. Neurons in the overlapping region are exposed to a field with an envelope amplitude that is modulated periodically at the difference frequency $\Delta f = f_1 - f_2$ (within the normal neural activity frequency range). It has been shown that the amplitude modulated kHz electric field drives neural activity at Δf [8], via a nonlinear mechanism-potentially involving nonlinear frequency mixing [22] associated with ion channels' signal rectification [12,23] and/or excitatory-inhibitory neural circuit dynamics [15,23].

Recent work applied TI stimulation with biphasic square (rather than sinusoidal) waves in the study of epilepsy [24,25]. Here, it was shown that this TI is able to successfully induce hippocampal ripples (150–250 Hz) in healthy mice, and suppress hippocampal epileptogenic biomarkers in mice with an induced epileptic state [24]. TI stimulation via biphasic square waves has additionally been demonstrated in a sleep apnea treatment in humans [26]. Crucially, the summation of two biphasic square waves, used in these studies, does not result in a waveform that is amplitude-modulated at Δf. Instead, it creates a waveform that has a pulse-width that is periodically modulated at Δf (Fig. 1A). Thus, the key question of whether kHz electric fields with a fixed envelope amplitude, but a pulse-width that changes periodically at frequencies within the normal neural range, can drive neural activity, emerges. Thus far, no direct evidence that pulse-width modulated-TI (PWM-TI) can drive neural activity at Δf has been presented. Furthermore, the efficiency and mechanisms of such a neuromodulatory approach are unknown.

Here we use ex-vivo single-cell electrophysiology and in-vivo neural circuit calcium imaging, to test the concept of PWM-TI stimulation brain stimulation (Fig. 1B–C). Specifically, we aim to assess whether PWM-TI can drive neural activity at Δf, and examine the neural response in comparison to conventional (i.e., sinusoidal-waveform) TI stimulation. We focus on the neural response when the applied electric fields have similar amplitudes resulting in a full PWM. An analysis of PWM-TI's spatial distribution was included in the original article [24]. We show that TI neuromodulation via square kHz electric fields drives neural activity at the difference frequency at a comparable efficiency to traditional sinusoidal TI stimulation (henceforth referred to as simply TI), suggesting that it is a viable method for non-invasive DBS. We then use computational modelling to show that the neuromodulation mechanism may involve the conversion of the applied PWM electric fields to AM transmembrane depolarization due to the intrinsic "low-pass filtering" property of the neural membrane.

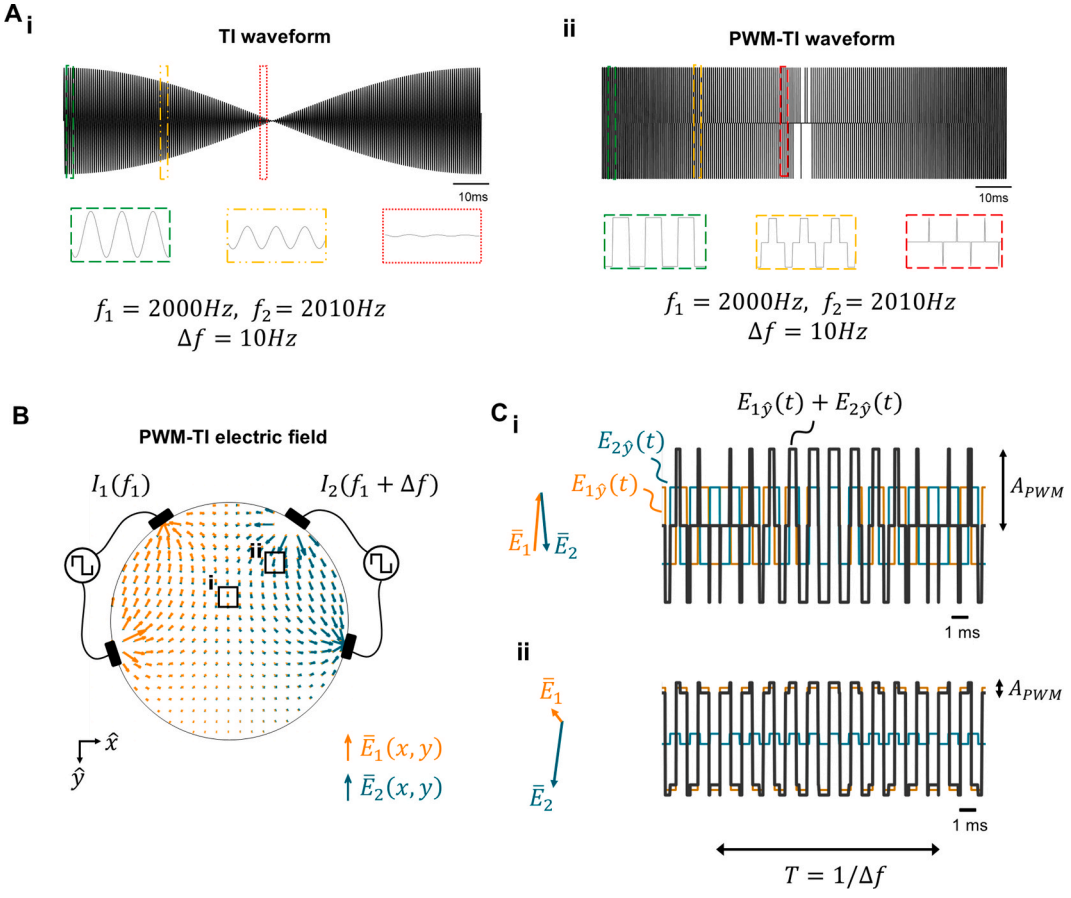


Fig. 1. PWM-TI concept.
A. i. TI stimulation via a superposition of two sinusoidal waveforms showing amplitude modulation.
ii. PWM-TI via a superposition of two square waveforms showing pulse-width modulation and constant envelope amplitude.
B. Head schematic showing PWM-TI concept for focused deep brain stimulation. Electric field vectors $\overline{E}_1(x,y)$ (orange) and $\overline{E}_2(x,y)$ (teal) resulting from the application of biphasic kHz square currents I_1 and I_2.
C. Zoom view of the time-domain PWM waveforms of the electric field amplitudes $E_{1\hat{y}}(t)$ and $E_{2\hat{y}}(t)$ along the $\hat{y}$ direction (normalized to maximum), for electric field vectors $\overline{E}_1$ (orange) and $\overline{E}_2$ (teal) respectively, in the regions indicated in B. Also shown is the superposition of the two fields ($E_{1\hat{y}}(t) + E_{2\hat{y}}(t)$) (black), i.e., the expected electric field in that region, showing i. a large pulse-width modulation amplitude (A_{PWM}) where $\overline{E}_1$ and $\overline{E}_2$ overlap fully, and ii. a small A_{PWM} where they do not.

2. Material and methods

Mice were housed in standard cages in the Imperial College London animal facility, with ad libitum food and water, a controlled light-dark cycle environment, and standard monitoring by veterinary staff. The Imperial College London's Animal Welfare and Ethical Review Body approved all animal procedures, and all experiments were performed in accordance with relevant regulations/according to the United Kingdom Animals (Scientific Procedures) Act 1986.

2.1. Ex-vivo single cell patch-clamp recording

2.1.1. Brain slice preparation

Experiments were performed on L2/3 cortical neurons from male C57BL/6 mice, aged between 4 and 7 weeks. Mice were anaesthetised using 100 mg/kg ketamine/10 mg/kg xylazine and transcardially perfused with 0–5 °C carbogenated dissection artificial cerebrospinal fluid (aCSF) containing (in mM): 108 C5H14ClNO, 3 KCl, 26 NaHCO3, 1.25 NaH2PO4, 25 Dextrose, 3 C_3H_3NaO, 1 $Mgcl_2$, and 2 $CaCl_2$. 350-μm-thick coronal slices surrounding the somatosensory cortex were prepared using a Vibratome (Campden Instruments LTD, Loughborough, UK). Following sectioning, the slices were left to recover for 2–4 h at room temperature in carbogenated bath aCSF containing (in mM): 120 NaCl, 3 KCl, 23 NaHCO3, 1.25 NaH2PO4, 1 $Mgcl_2$, and 2 $CaCl_2$. Following recovery, slices were placed in the recording chamber of the electrophysiology rig and held down using a harp (Multi Channel Systems, Reutlingen, Germany). The recording chamber was continually perfused with carbogenated bath aCSF throughout the experiment.

2.1.2. Waveforms

PWM-TI stimulation was created by summation of two constant amplitude biphasic square waveforms with duty cycles of 50 %, and frequencies of 2 kHz and 2.01 kHz. The resulting waveform is a constant envelope amplitude, biphasic square waveform with a frequency equal to 2.005 kHz, which has a pulse-width that changes periodically at the difference frequency (10 Hz). The inter-pulse interval (IPI) of the signal is equal to the period of the waveform (~0.5 ms). When the signal is fully constructive, the waveform has a symmetrical biphasic pulse-width equal to 50 % of the IPI (~0.25 ms). When the signal is fully destructive, the waveform has a symmetric biphasic pulse-width equal to 0 % of the IPI (0 ms). When the signal is half constructive and half destructive, the waveform has a symmetrical biphasic pulse-width equal to 25 % of the IPI (~0.125 ms).

Sinusoidal TI stimulation was created by summation of two biphasic sinusoidal waveforms with frequencies of 2 kHz and 2.01 kHz as previously described [8]. Traditional AC stimulation at the difference frequency was a 10 Hz biphasic sinusoidal waveform. A no stimulation (baseline) was recorded before each stimulation period. All waveforms were created in MATLAB with a sampling rate of 250 kHz. The biphasic bipolar square pulse waveform with decreasing pulse-widths was created with pulse-widths ranging from 50 ms to 0.012 ms.

2.1.3. Electrical stimulation

Electrical stimulation was applied through a single electrode pair. A 0.25 mm diameter platinum wire stimulating electrode (VWR, UK) was positioned just touching the slice, 50–100 μm from the recorded neuron on L2/3 cortex, before commencement of whole cell patch clamp recordings. We did not confirm the cell type, but based on the morphology, we estimated that the patched neurons were pyramidal cells. The return stimulation electrode consisting of two 2 x 2mm Ag/AgCl pellet electrodes (VWR, UK) in a y-shape configuration, was placed in the bath (ventral side of the slice). Electrical stimulation was delivered using a custom-written MATLAB GUI via a DAQ (USB-6216 BNC; National Instruments, Newbury, UK) and constant current isolator (LCI1107; Soterix Medical Inc, Woodbridge, NJ, USA). Each stimulation was applied for 5 s with 0.5 s ramp-up and 0.5 s ramp-down period, with a 5 s stimulation-free period between consecutive stimulations. Stimulation current steps were 0.1 mA (current density step: 0.05 mA/mm^2). Current density was estimated by dividing the applied current amplitude by the exposed surface area of the stimulation electrodes. The cylinder shape wire electrode had a radius $r = 0.125mm$ and an exposed hight $h = 5mm$, resulting in an exposed surface area $S \approx 4mm^2$ ($S = \pi r^2 + 2\pi rh$).

2.1.4. Whole cell patch clamp recordings

Patch electrodes were pulled from filamented thin-walled borosilicate glass capillaries using a horizontal Flaming–Brown micropipette puller (P1000; Sutter Instruments, Novato, CA, USA). Starting electrode tip resistance ranged from 5 to 8 MΩ. Patch electrodes were filled with internal solution containing (in mM): 130 $KMeSO_4$, 8 NaCl, 2 KH_2PO_4, 2 Dextrose and 10 HEPES. Whole cell patch clamp recordings were taken in current clamp mode (no holding current) using an amplifier (MultiClamp 700B; Molecular Devices Ltd, Wokingham, UK) and digitiser (Digidata 1550b; Molecular Devices Ltd), and data were acquired using pClamp software (Molecular Devices Ltd) with a sampling rate of 100 kHz. The stimulation electrode was 50–100 μm from the recorded neuron in the coronal plane. Following successful break-in and before each electrical stimulation, a membrane test was run on the cell to gather membrane statistics. Furthermore, a protocol comprising of current steps increasing in amplitude by 50 pA was run, to determine viability of the cell.

2.1.5. Patch-clamp data analysis

All analysis was done on membrane potential traces recorded during the 4 s stimulation period (with ramp up and ramp down periods removed), unless otherwise stated. Power spectral density (PSD) was computed using the multitaper method and normalized to the maximum PSD value (normalized PSD). To determine whether magnitude of polarisation at the Δf was significant, the difference in PSD at the frequency of interest compared to noise was computed by applying a linear fit to the log transform of the normalized PSD (fit was done across Δf $+/-5$ Hz) and calculating the difference from this fit/the noise floor of the PSD (Δ normalized PSD). Threshold for PWM-TI and TI stimulation was defined as the lowest applied current amplitude required to evoke an action potential (AP) train with at least three APs significantly ($p < 0.05$, Rayleigh test) phase locked to the subthreshold oscillation at Δf. Thresholds were normalized to threshold for traditional stimulation at Δf (i.e., no TI), which was determined in the same way, except with APs being significantly phase locked to the extracellular stimulation artifact at Δf. To calculate subthreshold oscillation amplitude in the time domain, the membrane potential trace in response to the maximum stimulation amplitude that had no APs was taken. The signals were filtered using a high-pass filter (Butterworth; 1 Hz, order 3) and a low-pass filter (Butterworth; 50 Hz, order 5) to remove DC shift and stimulation artifact. The average stimulation-induced subthreshold oscillation amplitude for each neuron was computed by computing root mean square (RMS) of the middle 1s of the filtered trace.

Phase difference between evoked subthreshold membrane polarization (PWM-TI vs TI), or between evoked subthreshold membrane polarization (PWM-TI or TI) and stimulation (stimulation artifact), was calculated. The signals were filtered using a high-pass filter (Butterworth; 1 Hz, order 3) and a low-pass filter (Butterworth; 50 Hz, order 5) and then Hilbert transformed (for evoked subthreshold polarization). High-pass filtered traces were Hilbert transformed, and then bandpass filtered around Δf (Bandwidth; 2 Hz, order 4) (for stimulation). The phase difference (angle) was then calculated as the difference in instantaneous phase of the two signals, and the circular mean instantaneous phase difference was calculated for each neuron.

For all analysis of subthreshold neural activity in the frequency and time domains, only neural recordings during stimulation where the neuron did not exhibit a suprathreshold response were included, to

ensure that the values being obtained were representative of purely subthreshold neural polarisation for that neuron.

2.2. In-vivo widefield calcium imaging

2.2.1. Surgical procedure

Male (n = 6) and female (n = 4) GCaMP6s mice (2–4 months old) were anaesthetised with 2–3% (vol/vol) isoflurane in oxygen and received a dose of carprofen (0.1 mg/g), buprenorphine (0.1 mg/kg), and dexamethasone (0.1 ml) subcutaneously at the start of the surgery. The animal was head-fixed in a stereotaxic frame, and the scalp removed. The skull was covered with a thin layer of cyanoacrylate glue (Superglue Brush on, Loctite), and transparent nail polish to make the bone transparent, and thus enable imaging through the intact skull. A custom-made headbar was attached to the skull with clear dental cement (Paladur) mixed with charcoal. Two holes (0.5 mm diameter) were drilled through the skull down to dura in the V1 visual area (AP -3.5, ML +1.25 and AP -3.5, ML +3.25 mm). Two custom-made electrodes (platinum-iridium, 0.25 mm diameter, Alfa Aesar) were placed in the holes, glued to the skull, and fixed to the headbar with cement. The skull area and electrodes were covered with another layer of nail polish. Mice received carprofen in water for two days post-surgery and were left to recover for 6–7 days before experiments.

2.2.2. Imaging

Widefield calcium imaging was done using a custom tandem-lens epifluorescence macroscope, as previously described [27]. Alternating 405 and 470 nm images were acquired at 50 Hz with a CMOS camera (GS3-U3-23S6, FLIR) for a 25 Hz imaging frequency per channel. The 405 and 470 nm channels measured hemodynamic and calcium signals respectively. Camera exposure per frame was limited to 10 ms and offset by 5 ms relative to LED onset, to limit crosstalk between the two channels. Camera, LEDs and stimulation were controlled by and synchronised with TTL pulses programmed in WaveSurfer software (HMMI Janelia).

Animals were imaged under light anaesthesia (0.5 % vol/vol isoflurane in oxygen), with the order of recordings randomised. Each individual recording was repeated three times and lasted 62 s: 20 s of baseline, 22 s of stimulation (1 s ramp up, 20 s full stimulation amplitude, 1 s ramp down), and 20 s of post stimulation activity.

2.2.3. Electrical stimulation

Electrical stimulation was delivered as in ex-vivo brain slice experiments but through two electrodes pairs applied by two current sources (LCI1107; Soterix Medical Inc), with phases $\varphi_1 = 0^\circ$ and $\varphi_2 = 180^\circ$. Additionally, auditory transformers (L1440-LN-B, Hammond Manufacturing, Basingstoke, UK) were used to remove noise and DC shifts, and to ensure extra channel isolation. Each stimulation trial lasted 22s, including 1 s current ramp up, 20 s full stimulation amplitude, and 1 s current ramp down. The inter stimulation interval was 20 s. During experiments, animals were connected to the stimulators via implanted sockets and return electrodes placed on shaved animal cheeks covered with electrode gel (SignaGel, Parker Laboratories, Fairfield, NJ, USA). The return electrodes consisted of ~3 x 3 mm conductive copper tape electrodes (RS Components, London, UK) connected to 26 AWG Teflon-coated silver wires (WPI, Hitchin, UK).

Reported current densities were computed by dividing the applied current amplitude by the cross-sectional area of the stimulation electrode. We used sufficiently low Δf (<1 Hz) to account for the low temporal resolution of the calcium imaging. In all imaging experiments, amplitude modulation of TI was temporally aligned with constructive interference of PWM-TI to allow for direct phase comparison between the two.

2.2.4. Widefield calcium imaging data analysis

All data was averaged across 3 repeat recordings and downsampled with a box-shaped kernel by a factor of 3 for a 384 × 400 pixels field of view (FOV). For each animal, images were registered between days to the animal reference frame by applying linear rigid transformation (using NoRMCorre package [28]). The images were rotated to ensure midline is placed symmetrically in the image, with angle per animal calculated by manually selecting two points on the midline of the reference image. All images were further registered to the scaled 2D top cortical projection of the Allen Brain Atlas reference space, using manually selected reference points (base of olfactory bulb, lambda). Each combined recording was deinterleaved to split the data into the 405 and 470 (nm) channels. The 405 and 470 channels were individually normalized at the pixel level to the median fluorescence of the first 20 s of each recording (F_0) for dF/F traces ($\frac{dF}{F} = \left(\frac{F-F_0}{F_0}\right)$), representing change in fluorescence relative to baseline. The 405 nm channel was temporally smoothed using moving average window of 400 ms and then subtracted from the 470 nm channel to calculate the final reported dF/F, i.e. change in calcium fluorescence free of hemodynamic artefacts. The resulting data was temporally smoothed with a moving average of 200 ms at a single pixel level and detrended using a robust 3rd-order polynomial fitting method ([29]; 10/2019 software version), which excluded events of >10 % dF/F amplitude from the fit.

Regions of interest (ROIs) were ~0.5 x 0.5 mm large (18 x 18 pixels) and was positioned between the two cortical electrodes, where maximum amplitude modulation is expected, custom for each animal. Example traces show mean dF/F activity from ROI for all animals (n = 10; for all statistics). PSD plots were computed on the 20 s of baseline and stimulation periods using the multitaper method. PSD values between original frequency bins were interpolated, and the plots were smoothed using linear least squares with a 1st degree polynomial model method.

Stimulation evoked dF/F (%) at the frequency of interest (FOI), was computed by first bandpass filtering the dF/F traces with a bandwidth of 0.05 Hz around FOI (e.g. for 0.5 Hz, window = 0.475–0.525 Hz), and then computing the percentage difference between the stimulation period and a 20 s stimulation-free period preceding it. Current threshold per condition (TI or PWM-TI) was determined as the minimum amount of current density needed to induce a significant increase in dF/F (%) at a specified frequency. Onset response was quantified as the maximum dF/F amplitude recorded during and immediately after the current ramp up (1 s ramp up time + 2 s of full stimulation). Significance of evoked dF/F was established by comparing them to the spontaneous level.

Mixed-effect linear models (lmer function, Matlab) were fitted to analyse responses, with current amplitude and condition type as fixed effects and mouse ID as a random effect. Condition and current were treated as categorical variables, with reference coding scheme (lowest current density and standard TI as references).

Phase difference between responses evoked by PWM-TI vs TI at Δf was calculated on stimulation traces that were first bandpass filtered around FOI (bandwidth = 0.1 Hz) and then Hilbert transformed. The phase difference (angle) between them was then calculated as difference in instantaneous phase of the two signals.

2.3. Computational modelling

All modelling was performed in the NEURON environment (NEURON 7.8.1) [30,31].

Multi-compartment modelling was performed using a biophysically realistic layer 2/3 pyramidal neuron ('L2/3 PC') (created by Ref. [32]). The neuron model was optimised by the authors for testing the effect of electrical stimulation. The four "clones" of the model neuron with different morphologies were also used when multiple cells were needed for statistical purposes [32]. The models are available at ModelDB (repository number 241165). The neuron models are shown in Fig. 4a. The Hodgkin-Huxley model parameters used are as originally described in Ref. [32,33], i.e., no modifications were made to the models. All

recordings were taken at the soma (the reported characteristics of the neural response to TI and PWM-TI as recorded in the axon were not different).

Stimulation waveforms were created as in 'Waveforms'. Each stimulation was applied for 1s with a 0.5 s ramp-up and 0.5 s ramp-down period, with a 100 ms stimulation-free period before stimulation. Simulations were run with a sampling rate of 250 kHz (4 μs stime step). The extracellular electric stimulation was applied as in the original paper [32]. Briefly, uniform electric fields were applied downwards relative to the somatodendritic axis of the neuron, and thus pointing inward from, and perpendicular to, the surface of the cortex- consistent with the experiments. The extracellular potential Ve(x,y,z) at each model compartment (x,y,z), was computed using the compartment's location and orientation in spherical coordinates relative to the soma that was set to ground (i.e., V = 0), using $Ve(x,y,z) = -|E| \cdot (x\sin\theta\cos\varphi + y\sin\theta\sin\varphi + z\cos\theta)$, where θ is the polar angle and ∅ the azimuthal angle in the spherical coordinate. The electric potential was then scaled by the specific current amplitude of the PWM-TI and TI waveforms over time. The extracellular potential was applied to the model compartments using NEURON's extracellular mechanism. To simulate the effect of the passive membrane, in a subset of simulations, we set the conductance of all the voltage gated ion channels to 0, thereby computationally blocking their conductance.

A single compartment model composed of a resistance representing the passive leak resistance/conductance, and a capacitance representing the membrane capacitance was also used. Intracellular current stimulation with PWM-TI and TI was applied to this neuron. Time constant (τ) of the single compartment NEURON model was altered within the bounds of physiological neuronal time constants (1–100 ms) (based on the literature, data obtained at https://neuroelectro.org), by changing the passive conductance. Specific membrane capacitance was fixed at 1μf/cm2.

2.3.1. Computational modelling data analysis

Threshold was defined as the current amplitude required to produce 1 AP. The threshold amplitude was determined to the nearest 1 V/m, and the measured thresholds for TI and PWM-TI were ~50–450 V/m. The thresholds for low frequency stimulation at Δf were 13.44 V/m (sinusoidal) and 12.03 V/m (square). To compute the amplitude of membrane potential activity at Δf, recordings were high-pass filtered (Butterworth; 2 Hz, order 3) to remove offset, and low-pass filtered (Butterworth; 20 Hz, order 4), and RMS amplitude was computed.

The depth of the amplitude modulation was computed by extracting the signals' envelope signals using Hilbert transform (abs(Hilbert), Matlab), and then dividing half the peak-to-peak amplitude of the envelope signals by half the peak-to-peak amplitude of the original signals.

2.4. General data analysis

All data was analysed in MATLAB (MATLAB 2019a, MATLAB 2021a, The MathWorks Inc.) except for linear mixed-effect model (LMM) fitting. Phase statistics were done using circular statistics toolbox in MATLAB [34]. LMM analysis was done in R using lme4 and emmeans packages.

2.4.1. Statistical analysis

All data in the text is mean ± SEM. Statistical tests are specified in the text, figure legends and supplementary tables.

2.4.2. For ex-vivo brain slice and computational modelling

All *t*-tests are two tailed unless stated. In all plots, the * notation represents a statistical significance that survived Bonferroni correction.

2.4.3. For widefield calcium imaging

Full statistics are shown in Tables S1–S3. *t*-tests are one-tailed for comparisons to zero/baseline and two-tailed for comparisons between conditions. In all plots, the * notation represents a statistical significance that survived Bonferroni-Holm correction.

3. Results

3.1. PWM-TI stimulation of single neurons investigated via ex-vivo patch-clamp recording

We first determined whether PWM-TI can depolarize the neural membrane potential at the difference frequency (Δf). We applied two square waveform electric fields at slightly different kHz frequencies (f_1 = 2000 Hz, f_2 = 2010 Hz, Δf = 10 Hz) (Fig. 1B) simultaneously via one pair of electrodes to mouse brain slices and measured the transmembrane potential in individual neurons using a whole-cell patch-clamp recording (Fig. 2A). The square waveforms were symmetrical and biphasic (50 % duty cycle positive pulse and 50 % duty cycle negative pulse with equal amplitude), resulting in a kHz electric field with pulse-width modulation at Δf (Fig. 1Aii). To explore the efficiency of the PWM-TI stimulation relative to the traditional TI stimulation, we also applied the same amplitude electric fields but with sinusoidal waveforms (Fig. 1Ai). See Methods for details. We found that the PWM-TI stimulation evoked subthreshold membrane depolarization at Δf (Fig. 2C; note the PSDs at the applied frequencies are stimulation artefact) (Δ normalized power spectrum density (PSD): 0.0014 ± 4.37e-04, p = 0.0054; one tailed one sample *t*-test). The average root mean square (RMS) amplitude of this evoked oscillatory polarisation was (~40 %) larger during PWM-TI compared to TI, when the applied current density was the same (0.67 ± 0.081 vs 0.40 ± 0.057 mV, p = 0.010; paired *t*-test) (Fig. 2Di–ii).

There was a small phase difference (8.73 ± 3.42°) between the oscillations evoked by PWM-TI and TI (Fig. 2Diii). At higher current densities, the PWM-TI evoked action potentials (APs) at Δf (Fig. 2Ei). The threshold for evoking AP activity at Δf was slightly lower than for traditional TI stimulation and was approximately 1–1.5 times larger than the threshold for traditional alternating current (AC) stimulation at Δf (normalized AP threshold: PWM-TI, 1.24 ± 0.21; TI, 1.55 ± 0.29; p = 0.016; paired *t*-test) (Fig. 2Eii). PWM-TI and TI-evoked subthreshold activity are positively phase-shifted relative to the constructive phase of the waveforms (PWM-TI: 73.00 ± 2.95°, TI: 66.11 ± 4.30°) (Figs. S1A–B), suggesting that the polarisation follows the constructive phase. The phase of the PWM-TI and TI evoked subthreshold oscillatory polarisation relative to the stimulation was consistent across neurons (PWM-TI: p = 5.03e-08, TI: p = 1.59e-07, Rayleigh test for non-uniform distribution) (Fig. S1B), evident in the large phase resultants (PWM-TI: 0.83 ± 0.058, TI: 0.86 ± 0.025). PWM-TI and TI-evoked APs occur as subthreshold polarisation is peaking, as expected (Fig. S1C). Note, the PWM-TI stimulation artifact signal recorded by the patch-clamp apparatus is amplitude-modulated due to its low-pass filtering. During the stimulation-free periods, there was no change in Δf power (Δ normalized PSD: −0.0039 ± 0.0027, p = 0.90; one tailed one sample *t*-test), confirming that polarisation at this frequency is due to stimulation. These results suggest that PWM-TI can efficiently depolarize neurons at Δf, in a way that is comparable and perhaps slightly stronger than traditional TI.

3.2. PWM-TI stimulation of neural networks investigated via in-vivo calcium imaging

We next examined whether PWM-TI stimulation can drive circuit-level activity in-vivo. We applied two square electric fields at slightly different kHz frequencies (f_1 = 2000 Hz, f_2 = 2000.5 Hz, Δf = 0.5 Hz) simultaneously via two pairs of electrodes to the cortex of head-fixed, lightly anaesthetised GCaMP6 mice [35], and measured the evoked response in the overlap region of interest (ROI) using widefield calcium imaging (Fig. 3A). Here we used a lower Δf to account for the slow kinetics of the calcium indicators. We found that PWM-TI evokes reliable network-level oscillations at both Δf and its harmonic, $2\Delta f$ (Fig. 3B). In

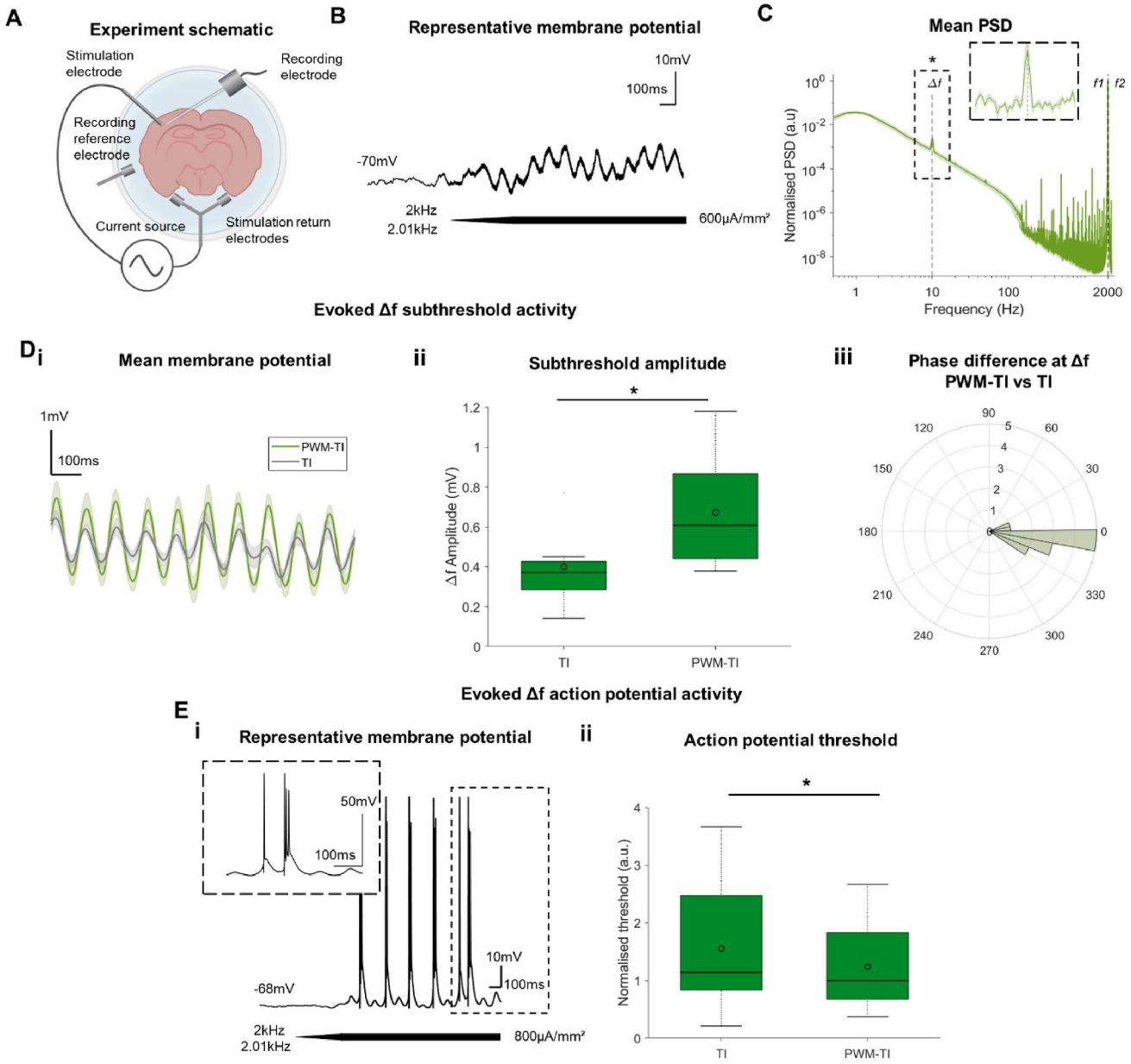


Fig. 2. PWM-TI depolarizes neurons at the difference frequency ex-vivo.

A. Schematic showing patch clamp with extracellular stimulation experiment set up. Extracellular stimulation is applied via one electrode pair, $f_1 = 2000$ Hz and $f_2 = 2010$ Hz ($\Delta f = 10$ Hz) for all plots.

B. Representative membrane potential trace recorded from a cortical neuron during subthreshold PWM-TI at 600 μA/mm^2 current density. Trace is filtered with a 500 Hz low-pass Butterworth filter to remove stimulation artifact.

C. Normalized power spectral density (PSD) (mean ± SEM) of the neural membrane potential when neurons are stimulated with the maximum current density that evoked a subthreshold response in all neurons. Zoom view pertaining to region inside dashed box (Δ normalized PSD). Stimulation as in B. PSD normalized to maximum value. One sample one tailed *t*-test, * = $p < 0.05$. Note the PSDs at f_1 and f_2 (i.e., 2000 Hz and 2010 Hz) are stimulation artefact.

D. i. Membrane potential during stimulation with TI (grey) and PWM-TI (green), showing mean (±SEM) subthreshold oscillation at Δf of 10 Hz. Trace is low-pass filtered at 20 Hz. ii. Boxplot showing the root mean square (RMS) amplitude of subthreshold oscillations in (i). Two tailed paired *t*-test, * = $p < 0.05$ iii. Polar histogram (displaying count) showing the phase difference between PWM-TI and TI. For plots in D, for each neuron, the maximum current density that was still subthreshold for both stimulation conditions was taken.

E. i. As in B, but for suprathreshold stimulation at 800 μA/mm^2. ii. Boxplot showing the normalized threshold for action potential (AP) generation, for TI and PWM-TI. Thresholds normalized to the threshold for AP generation when the cell is stimulated with a sinusoidal waveform at Δf (10 Hz). Two tailed paired *t*-test, * = $p < 0.05$.

All boxplots showing median (line), mean (circle) and interquartile range (IQR). Whiskers extend to the most extreme data points not considered outliers. Number of neurons/slices = 12 for all plots.

order to find the network-level stimulation threshold, the same stimulation was applied at increasing current intensities for both TI and PWM-TI. The minimum current density required to induce Δf oscillations was lower for PWM-TI compared to TI, with thresholds established at 2 mA/mm^2 and 2.5 mA/mm^2 respectively (20 % difference; Fig. 3Ci; see Table S1 for full statistics). The overall increase in the amplitude of Δf oscillations under PWM-TI stimulation was slightly larger than under TI stimulation (linear mixed-effect model (LMM): current density: F =

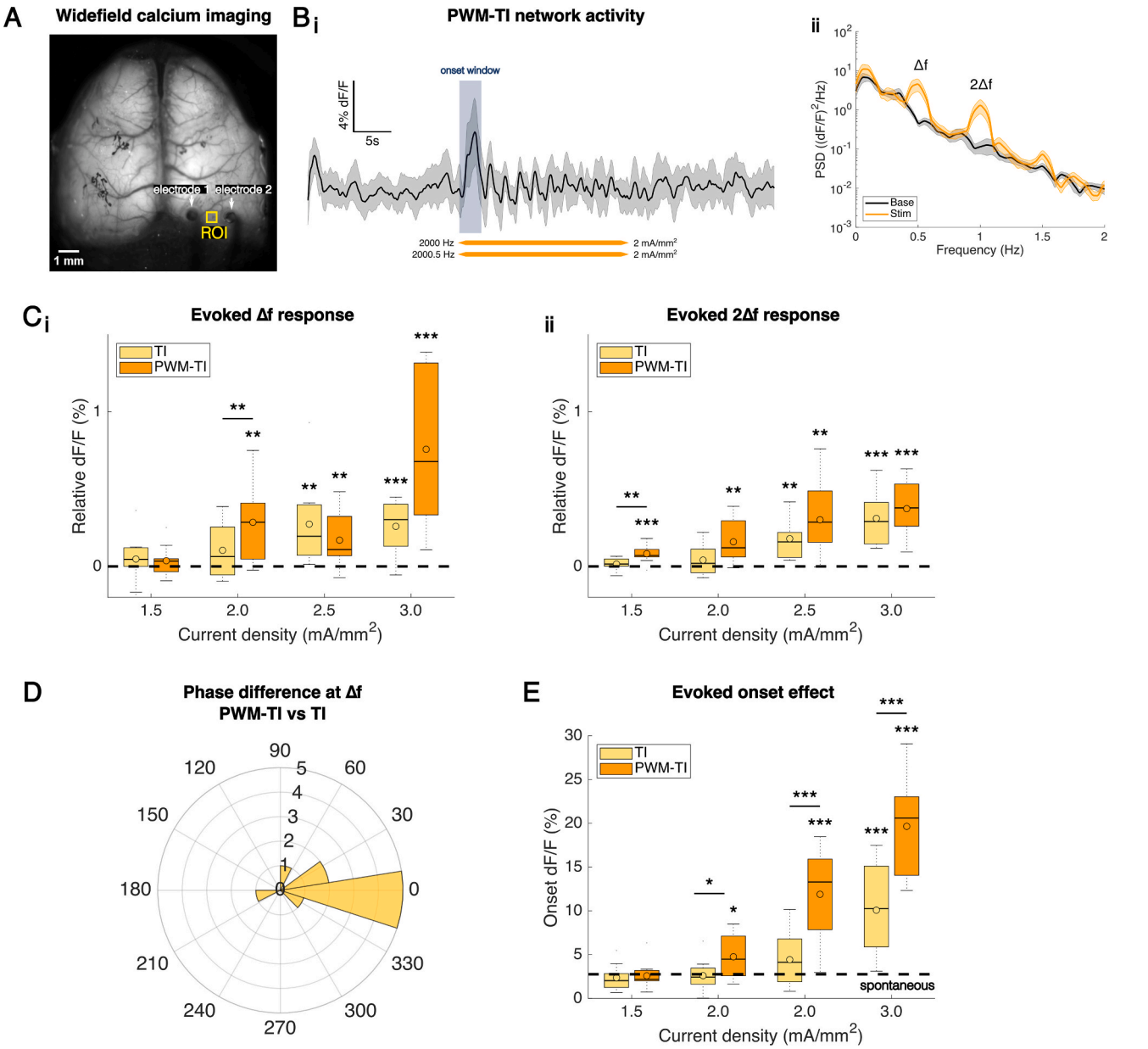


Fig. 3. PWM-TI drives cortical calcium activity at the difference frequency in-vivo.

A. Example field of view (FOV) for widefield calcium imaging experiments in GCaMP6s mice. A region of interest (ROI) used for subsequent analysis is located between two implanted stimulating electrodes. Two corresponding return electrodes were placed on the animal cheeks.

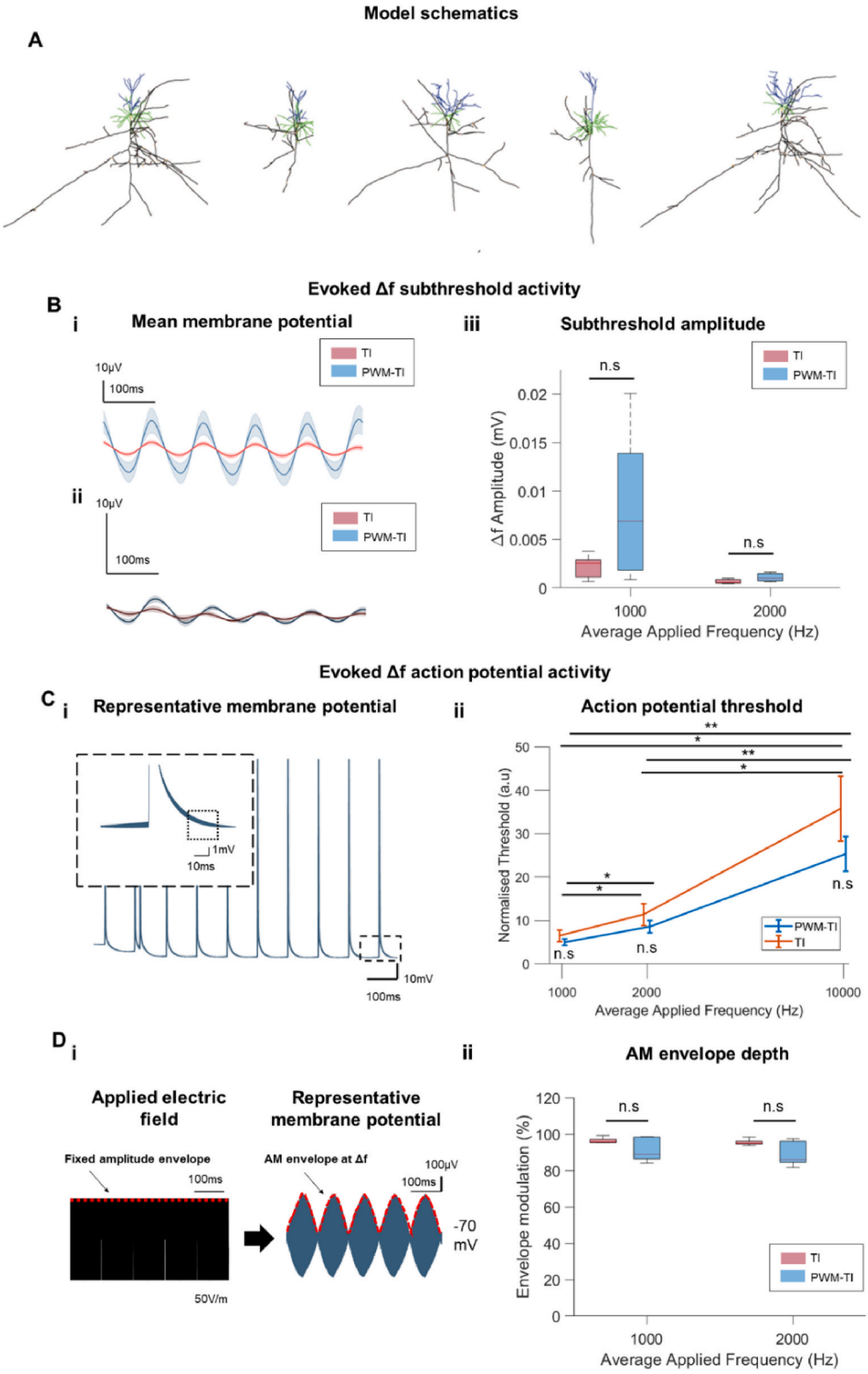
B. i. Mean ROI calcium traces during PWM-TI stimulation with 2000 Hz and 2000.5 Hz ($\Delta f = 0.5$ Hz) at 2 mA/mm^2 current density per electrode. Each stimulation condition consisted of 20 s of baseline activity, 1 s ramp up, 20 s of stimulation time, 1 s ramp down, and 20 s of post stimulation time. Blue window indicates the onset response window used to quantify the onset effect in E. Mean ± SD. ii. Mean power spectral density (PSD) of baseline (0–20 s) and stimulation (21–41 s) traces shown in Bi. Mean ± SEM.

C. i. Network responses at Δf at increasing current densities for TI and PWM-TI. The threshold for evoking reliable oscillation was lower for PWM-TI (current density of 2 mA/mm^2 per electrode) than for standard TI (2.5 mA/mm^2). Current, condition (TI vs PWM-TI) and interaction between the two are significant predictors of the response (see main text for details). Horizontal dashed line indicates baseline activity level. * <0.05, ** <0.01, *** 0.001, Bonferroni-Holm corrected for multiple comparisons within each condition. ii. As in Ci but at 2 Δf. Similarly, the threshold for evoking response was lower for PWM-TI (3 mA/mm^2) than for standard TI (5 mA/mm^2). Both current and condition are significant predictors of the evoked response (see main text for details).

D. Polar histogram (displaying count) showing the Δf oscillations induced by PWM-TI are in-phase with the Δf oscillations induced by TI (current density of 2 mA/mm^2; non-uniform distribution: p = 0.0078, Rayleigh test; phase not different from zero: h = 0, μ = 6.8°, CI [-30.1°, 44.0°], one-sample test for the mean angle, n = 10 for both).

E. Onset response, i.e., maximum dF/F amplitude at stimulation onset, is stronger for PWM-TI than for TI at the same current densities. Current, and interaction between the two are all significant predictors of the onset magnitude (see main text for details). Horizontal dashed line indicates mean onset amplitude during spontaneous recordings.

All boxplots showing median (line), mean (circle) and interquartile range (IQR). Whiskers extend to the most extreme data points not considered outliers. Number of animals = 10 for all plots.



(caption on next page)

Fig. 4. Modelling of PWM-TI neural stimulation revealing AM membrane depolarization.
A. Schematic showing the five biophysically realistic layer 2/3 pyramidal neuron computational models [32] used in subsequent investigations. All stimulation is extracellular.
B. i. Mean (±SEM) membrane potential during stimulation with TI (red) and PWM-TI (blue), $f_1 = 1000$ and $f_2 = 1010$ Hz ($\Delta f = 10$ Hz), showing subthreshold oscillation at Δf. Electric field strength of 50 V/m. Trace is low-pass filtered at 20 Hz. ii. As in i for $f_1 = 2000$ and $f_2 = 2010$ Hz ($\Delta f = 10$ Hz). iii. Boxplot showing the root mean square (RMS) amplitude of subthreshold oscillations in i and ii. n. s = $p > 0.0025$ (Bonferroni corrected p-value), two-tailed paired *t*-test.
C. i. Representative membrane potential trace during stimulation with a suprathreshold PWM-TI current, $f_1 = 2000$ Hz, $f_2 = 2010$ Hz. Left Zoom view of region inside dashed box. Electric field strength is 150 % above threshold. ii. Boxplot showing normalized threshold to evoke Action Potential (AP)s of TI and PWM-TI, across a range of applied frequencies. Δf across applied frequencies is 10 Hz. Threshold at each applied frequency normalized to threshold for evoking APs with low frequency stimulation at Δf for that stimulation type. * indicates a significant difference that survived Bonferroni correction. n. s = $p > 0.0167$ (Bonferroni-corrected p-value), * = $p < 0.05$, ** = $p < 0.005$, paired *t*-test for comparison between stimulation paradigms; repeated measures ANOVA with post-hoc paired *t*-test for comparison between applied frequencies.
D. i. Conversion of the constant amplitude PWM-TI waveform to an amplitude modulated membrane potential, $f_1 = 2000$ and $f_2 = 2010$ Hz ($\Delta f = 10$ Hz). ii. Boxplot showing percentage of envelope modulation for TI- and PWM-TI-induced subthreshold polarisation of the membrane potential, across applied frequencies. Electric field strength is 50 V/m for all conditions. Δf across applied frequencies is 10 Hz. n. s = $p > 0.025$ (Bonferroni-corrected p-value), paired *t*-test.
All boxplots show median (line), 25th (bottom edge) and 75th (top edge) percentiles. Whiskers extend to the most extreme data points not considered outliers. + indicates outliers. n = 5 different model neurons for all plots.

11.93, df = 3, p = 2.8e-06; stimulation condition: F = 6.30, df = 1, p = 0.015; interaction: F = 5.59, df = 3, p = 0.0018). The dependency on the evoked oscillations on the applied current density was consistent at $2\Delta f$, Fig. 3Cii (thresholds: 1.5 and 2.5 mA/mm^2 for PWM-TI and TI, 40 % reduction, see Table S2 for statistics; LMM: current density: F = 22.19, df = 3, p = 4.77e-10; stimulation condition, F = 10.67, df = 1, p = 0.0017; interaction term did not improve the model fit: $\chi 2 = 1.02$, p = 0.80).

The Δf oscillations induced by PWM-TI stimulation were consistently in-phase with the Δf oscillations induced by the TI stimulation (Fig. 3D; at 2 mA/mm^2; non-uniform distribution: p = 0.0078, Rayleigh test; phase not different from zero: h = 0, $\mu = 6.8°$, CI [-30.1°,44.0°], one-sample test for the mean angle). The stronger effect of PWM-TI was also reflected in a larger onset response compared to TI, across multiple current density amplitudes (see Table S3 for statistics; LMM: current density: F = 84.03, df = 3, p = < 2.2e16; stimulation condition: F = 62.89, df = 1, p = 4.72e-11; interaction: F = 12.86, df = 3, p = 1.18e-06). These results suggest that PWM-TI can evoke local oscillatory network activity at Δf with an efficiency that is similar to, and perhaps slightly stronger than, traditional TI.

3.3. Mechanism of PWM-TI stimulation investigated via computational modelling

Finally, we explored the mechanism by which PWM-TI stimulation depolarizes the neural membrane potential using computational modelling. We applied similar electric fields ($f_1 = 1000$ Hz, $f_2 = 1010$ Hz, $\Delta f = 10$ Hz; or $f_1 = 2000$ Hz, $f_2 = 2010$ Hz, $\Delta f = 10$ Hz) to realistic multi-compartment neural models [32], and quantified the evoked membrane potential. Fig. 4A shows a schematic of the five, layer 2/3 pyramidal neuron models used. We found that the PWM-TI stimulation evoked Δf subthreshold membrane depolarization with similar efficiency to traditional TI stimulation across applied frequencies (Fig. 4B), (PWM-TI, 0.0084 ± 5.51e-04 mV; TI, 0.0022 ± 0.0035 mV; p = 0.11 (1 kHz); PWM-TI, 0.0011 ± 1.02e-04 mV; TI, 0.0007 ± 0.0002 mV; p = 0.091 (2 kHz); paired-*t*-test, Bonferroni-corrected p-value = 0.025). The evoked Δf depolarization decreased with increasing kHz electric fields (1 kHz vs 2 kHz: PWM-TI, p = 0.022; TI: p = 0.023; paired *t*-test, Bonferroni-corrected p-value = 0.025). At higher electric field amplitudes, PWM-TI stimulation evoked Δf AP activity at a similar threshold to TI stimulation (Fig. 4C), (normalized AP threshold: PWM-TI, 4.97 ± 0.7; TI, 6.48 ± 1.38; p = 0.089 (1 kHz); PWM-TI, 8.63 ± 1.41; TI, 11.36 ± 2.5; p = 0.071 (2 kHz); PWM-TI, 25.33 ± 4.04; TI, 35.73 ± 7.47; p = 0.047 (10 kHz); paired *t*-test, Bonferroni-corrected p-value = 0.017). As before, the AP threshold values were normalized to the threshold for traditional AC stimulation at Δf (see Discussion for contextualization with experimental results which show lower relative thresholds).

We next explored the evoked membrane depolarization at the applied kHz frequencies (note, experimentally, electrophysiological signals at the applied frequencies are confounded by the strong stimulation artefact, rendering such exploration impossible). Interestingly, despite having a fixed envelope amplitude, we found that the kHz PWM-TI stimulation evoked kHz membrane depolarization with an envelope amplitude modulated at Δf (Fig. 4Di). The depth of the AM membrane depolarization evoked by PWM-TI stimulation was similar to that evoked by the TI stimulation (AM depth: PWM-TI: 91.32 ± 2.98 %, TI: 96.33 ± 0.72 %, p = 0.19 (1 kHz); AM depth: PWM-TI: 89.11 ± 3.09 %, TI: 95.35 ± 0.79 %, p = 0.16 (2 kHz); paired *t*-test, Bonferroni-corrected p-value = 0.025) (Fig. 4Dii). These results suggest the neuromodulation mechanism of PWM-TI stimulation involves a conversion to AM by the neural membrane, resulting in a similar membrane depolarization pattern to traditional TI stimulation.

Next, we sought to ask how the periodic change in the electric field pulse-width induces membrane depolarization with a periodic amplitude change. We hypothesized that the PWM to AM conversion is mediated by the low-pass filtering property of the cell membrane. To test this, we repeated the simulation in the neural model but without active ion channel conductance (i.e., ion channel conductance was set to zero) (Fig. 5A). We found that, indeed, stimulation with kHz electric fields with PWM at Δf, induced membrane depolarization with AM at Δf (Fig. 5B) (AM depth: 89.37 ± 3.49 %, p = 5.73e-09; two-sample *t*-test vs envelope of applied electric field). We found a similar PWM to AM conversion when we tested the depolarization across a simplified single-compartment neural model without active ion channels (i.e., a parallel R_mC_m circuit; R_m specific membrane resistance, C_m specific membrane capacitance) (Fig. 5C–D). The parallel R_mC_m causes the voltage to rise and fall more gradually than the stimulation pulse, attenuating the peak amplitude if the pulse-width is too short (Fig. 5E–F). The rising and falling time of the membrane is determined by its time constant $\tau_m = R_mC_m$, predicting weaker AM (attenuation happening at small pulse-widths) for cells with larger time constants. Accordingly, when τ_m of the simple model neuron is varied for a given pulse-width, the amplitude of the evoked membrane potential changes, with membrane potential amplitude decreasing as τ increases, as expected (Fig. 5F). These results suggest that the passive properties of the neuronal membrane are sufficient for PWM-TI stimulation to result in amplitude-modulated depolarization a process that depends on the time constant of the neuronal membrane.

4. Discussion

We reported the description and validation of a PWM-TI stimulation that uses multiple square kHz electric fields at slightly different frequencies, to generate an electric field with a pulse-width modulated at the difference frequency at the overlapping region. We showed that the PWM-TI stimulation strategy modulates neural activity at the difference

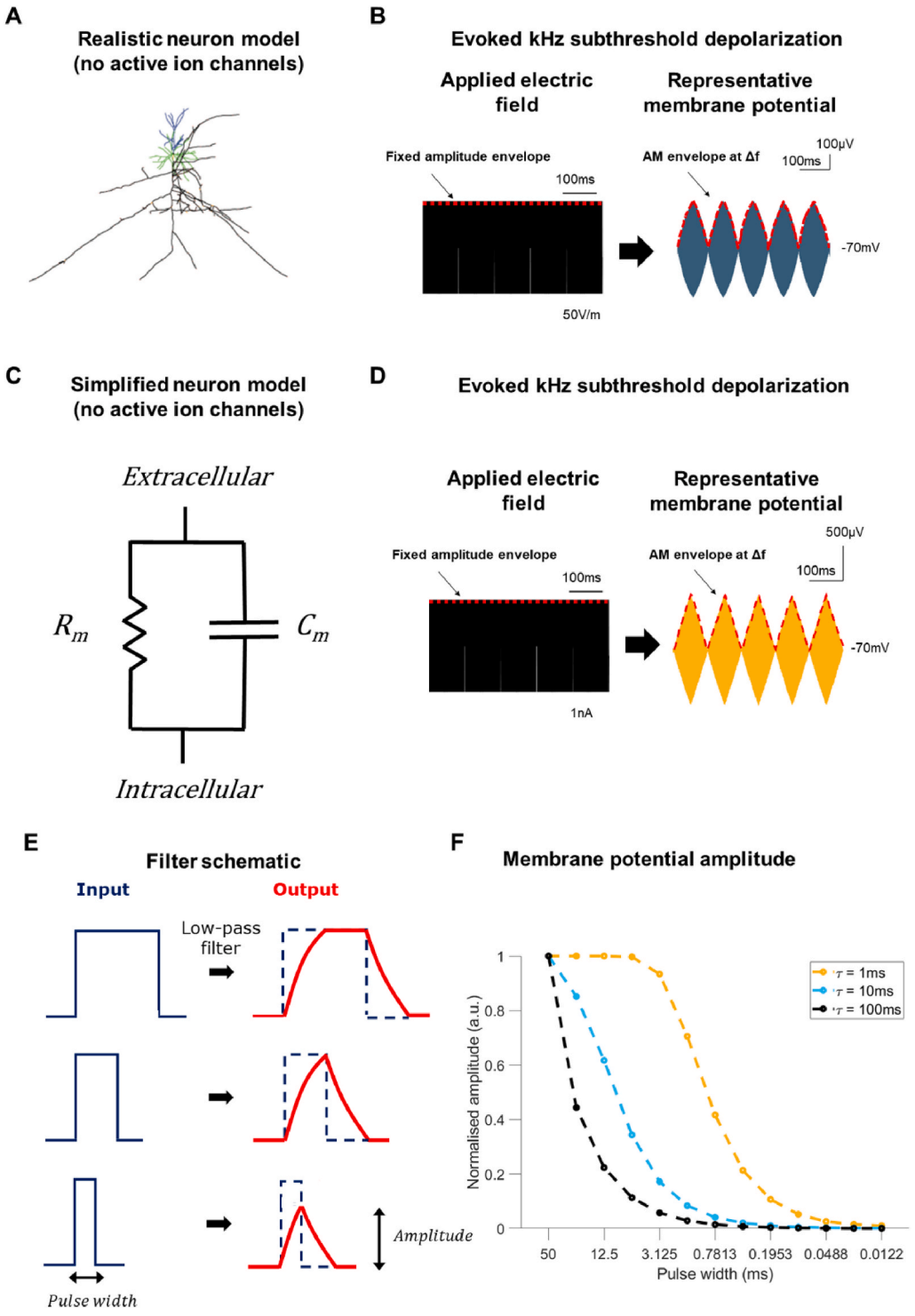


Fig. 5. Conversion of PWM stimulation to AM membrane depolarization originates fin the passive membrane low-pass filtering.
A. Schematic showing the biophysically realistic layer 2/3 pyramidal neuron computational model [32] used. Active ion channels are blocked, and stimulation is extracellular.
B. Conversion of the constant amplitude PWM-TI waveform to an amplitude modulated membrane potential, $f_1 = 2000$ and $f_2 = 2010$ Hz ($\Delta f = 10$ Hz) for the model in A.
C. Schematic showing the simple RC neuron computational model used. Stimulation is intracellular. Time constant (τ) is 1 ms.
D. Conversion of the constant amplitude PWM-TI waveform to an amplitude modulated membrane potential, $f_1 = 2000$ and $f_2 = 2010$ Hz ($\Delta f = 10$ Hz) for the model in C.
E. Schematic showing filtering of square current pulses by a low-pass filter leading to amplitude attenuation as pulse-width decreases.
F. Normalized amplitude of membrane potential depolarization induced by a train of biphasic bipolar square pulses vs pulse-width. Plot shows responses of simple model neurons (as in C) with different τ values. Plot showing peak to peak amplitude, normalized to the maximum peak to peak amplitude for each τ.

frequency, similar to traditional TI stimulation using sinusoidal kHz electric fields.

Our single-cell recordings show that both TI and PWM-TI neural stimulation involves the evocation of a subthreshold oscillation at the difference frequency Δf, evidence of a nonlinear frequency mixing depolarization mechanism [22], potentially due to rectification by the voltage-gated ion channels [12]. A linear depolarization mechanism would only generate oscillations at the applied frequencies without creating new frequency components. The induction of the second harmonics at $2\Delta f$ seen in the calcium imaging may also be attributed to nonlinear mixing [22], but could as well be an intrinsic property of the cortical network-level interactions.

The subthreshold depolarization induced by PWM-TI stimulation is first amplitude-modulated by the filtering of the passive membrane, rendering the subsequent active depolarization very similar to TI. A low pass filter forces a slower voltage ramp. If the voltage ramping time is shorter than the pulse duration, the induced peak voltage will be proportionally smaller. This simple principle may underpin the consistently reported strength-duration property of neurons, i.e., an inverse relationship between the stimulation pulse duration (below the chronaxie duration) and the strength of stimulation required to evoke an AP [36–40]. The dependency of the PWM to AM conversion on the membrane time constant may support strategies for PWM-TI with cell-type specificity. These strategies may utilize square waveforms with different duty cycles to generate more complex PWM-TI fields.

Our findings suggest that the neuromodulation efficiency of the PWM-TI stimulation is at least as good as the traditional TI stimulation. In some cases, PWM-TI showed slightly stronger stimulation (~40 % stronger subthreshold depolarization amplitude and ~20 % lower calcium signal threshold at the network level). This difference is likely explained by the fact that for a given set amplitude, the root mean square (RMS; corresponding to the energy) of a square waveform is larger than a sine wave. Specifically, the RMS of a square wave with an amplitude A is A, while the RMS of a sine wave with an amplitude A is $\sim A/\sqrt{2}$. Thus, the RMS of a square wave is $\sqrt{2}$ (≈1.4) times larger (i.e., ~40 % larger) than the RMS of a sine wave with the same amplitudes.

Our modelling results also show that the PWM-TI has a similar efficiency as TI. The lower efficiency at higher applied carrier frequencies is consistent with previous experimental findings [8], and may be attributed to the frequency-dependent depolarization of the membrane capacitance [41]. Yet, the modelling predicts a lower stimulation efficiency relative to conventional AC stimulation, than the experimental results. Specifically, our experimental results show that the efficiency of TI and PWM-TI in driving AP activity at Δf is approximately 1.5 times lower than conventional AC stimulation at Δf. In contrast, the computational results predict that TI and PWM-TI have 8–10 times lower efficiency than traditional AC stimulation at Δf. The neural models we used are commonly used to simulate conventional AC stimulation [32]. Yet, the homogenous electric field used in the model, and the lack of circuit input may increase the threshold compared to the experiment. Future studies combining experimental and computational investigations in the same neurons, with comparable field distributions and circuit input, might be able to better pinpoint this discrepancy in the computational models of TI.

Our report has limitations that should be addressed in future investigations. For example, here, we did not test the direct effect of square kHz stimulation without TI, as we and others experimentally tested for sinusoidal kHz stimulation [8,15]. In addition, we did not systematically test the effect of partial PWM modulation, nor whether changing the current ratio could steer the stimulation locus as in traditional TI. It is also important to note that, as with other forms of transcranial brain stimulation there may be some disparity between our study applying PWM-TI to the rodent brain, and any future human studies. These is in part due to rodent studies (such as ours) using electric field strengths that are larger than those used typically used in humans [42]. Regardless, the suprathreshold response we observed serves as a validation that PWM-TI is capable of strongly depolarising neurons at the difference frequency if a sufficient electric field strength is reached. In conclusion, PWM-TI is an effective neuromodulation approach to drive neural activity at the difference frequency, and the low-pass filtering of the neural membrane converts an envelope-fixed PWM-TI field to an amplitude-modulated membrane potential.

Funding

This work was supported by: UK Dementia Research Institute—an initiative funded by the Medical Research Council (NG, CL), Engineering and Physical Sciences Research Council, UK, EP/W004844/1 (NG), National Institute for Health and Care Research (NG), Imperial Biomedical Research Centre (NG), and the Medical Research Council (CL).

Data and materials availability

All data, code, and materials used in the analysis are available from the corresponding author upon request.

CRediT authorship contribution statement

Charlotte E. Luff: Conceptualization, Formal analysis, Investigation, Methodology, Project administration, Software, Visualization, Writing – original draft, Writing – review & editing. **Patrycja Dzialecka:** Conceptualization, Formal analysis, Investigation, Methodology, Software, Visualization, Writing – original draft, Writing – review & editing. **Emma Acerbo:** Conceptualization, Validation, Writing – review & editing. **Adam Williamson:** Conceptualization, Resources, Validation, Writing – review & editing. **Nir Grossman:** Conceptualization, Funding acquisition, Methodology, Supervision, Writing – original draft, Writing – review & editing.

Declaration of competing interest

NG. is an inventor of a patent on neuromodulation using temporal interference (TI) of kHz electric fields, assigned to MIT. NG is a co-founder of TI Solutions AG, a company committed to producing hardware and software solutions to support TI research.

Appendix A. Supplementary data

Supplementary data to this article can be found online at https://doi.org/10.1016/j.brs.2023.12.010.

References

[1] Benabid AL, Chabardes S, Mitrofanis J, Pollak P. Deep brain stimulation of the subthalamic nucleus for the treatment of Parkinson's disease. Lancet Neurol 2009;8 (1):67–81. S1474-4422(08)70291-6[pii]\r10.1016/S1474-4422(08)70291-6.

[2] Greenberg BD, Gabriels LA, Malone DA, Rezai AR, Friehs GM, Okun MS, Shapira NA, Foote KD, Cosyns PR, Kubu CS, Malloy PF, Salloway SP, Giftakis JE, Rise MT, Machado AG, Baker KB, Stypulkowski PH, Goodman WK, Rasmussen SA, Nuttin BJ. Deep brain stimulation of the ventral internal capsule/ventral striatum for obsessive-compulsive disorder: worldwide experience. Mol Psychiatr 2010;15 (1):64–79. https://doi.org/10.1038/mp.2008.55.

[3] Mayberg HS, Lozano AM, Voon V, McNeely HE, Seminowicz D, Hamani C, Schwalb JM, Kennedy SH. Deep brain stimulation for treatment-resistant depression. Neuron 2005;45(5):651–60. https://doi.org/10.1016/j.neuron.2005.02.014.

[4] Kuhn J, Hardenacke K, Lenartz D, Gruendler T, Ullsperger M, Bartsch C, Mai JK, Zilles K, Bauer A, Matusch a, Schulz R-J, Noreik M, Bührle CP, Maintz D, Woopen C, Häussermann P, Hellmich M, Klosterkötter J, Wiltfang J, Sturm V. Deep brain stimulation of the nucleus basalis of Meynert in Alzheimer's dementia. Mol Psychiatr 2014. https://doi.org/10.1038/mp.2014.32. November 2013, 1–8.

[5] Lozano AM, Fosdick L, Chakravarty MM, Leoutsakos J-M, Munro C, Oh E, Drake KE, Lyman CH, Rosenberg PB, Anderson WS, Tang-Wai DF, Pendergrass JC, Salloway S, Asaad WF, Ponce FA, Burke A, Sabbagh M, Wolk DA, Baltuch G,

Smith GS. A phase II study of Fornix deep brain stimulation in Mild Alzheimer's disease. J Alzheim Dis 2016;54(2):777–87. https://doi.org/10.3233/JAD-160017.
[6] Pikov V. Global market for implanted neuroprostheses. In: Kilgore K, editor. Implantable neuroprostheses for restoring function. first ed. Woodhead Publishing; 2015. p. 307–29. https://doi.org/10.1016/B978-1-78242-101-6.00014-8.
[7] Opitz A, Falchier A, Yan C-G, Yeagle EM, Linn GS, Megevand P, Thielscher A, Deborah AR, Milham MP, Mehta AD, Schroeder CE. Spatiotemporal structure of intracranial electric fields induced by transcranial electric stimulation in humans and nonhuman primates. Sci Rep 2016;6(1):31236. https://doi.org/10.1038/srep31236.
[8] Grossman N, Bono D, Dedic N, Kodandaramaiah SB, Rudenko A, Suk H-J, Cassara AM, Neufeld E, Kuster N, Tsai L-H, Pascual-Leone A, Boyden ES. Noninvasive deep brain stimulation via temporally interfering electric fields. Cell 2017;169(6). https://doi.org/10.1016/j.cell.2017.05.024. 1029–1041.e16.
[9] Violante IR, Alania K, Cassarà AM, Neufeld E, Acerbo E, Carron R, Williamson A, Kurtin DL, Rhodes E, Hampshire A, Kuster N, Boyden ES, Pascual-Leone A, Grossman N. Non-invasive temporal interference electrical stimulation of the human hippocampus. Nat Neurosci 2023. https://doi.org/10.1038/s41593-023-01456-8.
[10] Huang Y, Datta A, Parra LC. Optimization of interferential stimulation of the human brain with electrode arrays. J Neural Eng 2020;17(3):036023. https://doi.org/10.1088/1741-2552/ab92b3.
[11] Lee S, Lee C, Park J, Im C-H. Individually customized transcranial temporal interference stimulation for focused modulation of deep brain structures: a simulation study with different head models. Sci Rep 2020;10(1):11730. https://doi.org/10.1038/s41598-020-68660-5.
[12] Mirzakhalili E, Barra B, Capogrosso M, Lempka SF. Biophysics of temporal interference stimulation. Cell Systems 2020;11(6):557–572.e5. https://doi.org/10.1016/j.cels.2020.10.004.
[13] Rampersad S, Roig-Solvas B, Yarossi M, Kulkarni PP, Santarnecchi E, Dorval AD, Brooks DH. Prospects for transcranial temporal interference stimulation in humans: a computational study. Neuroimage 2019;202:116124.
[14] Wang B, Aberra AS, Grill WM, Peterchev AV. Responses of model cortical neurons to temporal interference stimulation and related transcranial alternating current stimulation modalities. J Neural Eng 2023;19(6):066047. https://doi.org/10.1088/1741-2552/acab30.
[15] Esmaeilpour Z, Kronberg G, Reato D, Parra LC, Bikson M. Temporal interference stimulation targets deep brain regions by modulating neural oscillations. Brain Stimul 2021;14(1):55–65. https://doi.org/10.1016/j.brs.2020.11.007.
[16] Sunshine MD, Cassarà AM, Neufeld E, Grossman N, Mareci TH, Otto KJ, Boyden ES, Fuller DD. Restoration of breathing after opioid overdose and spinal cord injury using temporal interference stimulation. Commun Biol 2021;4(1):107.
[17] Vieira PG, Krause MR, Pack CC. Temporal interference stimulation disrupts spike timing in the primate brain. 2023. bioRxiv 2023.09.25.559340. https://doi.org/10.1101/2023.09.25.559340.
[18] Ma R, Xia X, Zhang W, Lu Z, Wu Q, Cui J, Song H, Fan C, Chen X, Zha R. High gamma and beta temporal interference stimulation in the human motor cortex improves motor functions. Front Neurosci 2022;15:800436.
[19] Zhu Z, Xiong Y, Chen Y, Jiang Y, Qian Z, Lu J, Liu Y, Zhuang J. Temporal interference (ti) stimulation boosts functional connectivity in human motor cortex: a comparison study with transcranial direct current stimulation (tdcs). Neural Plasticity 2022:2022.
[20] Wessel MJ, Beanato E, Popa T, Windel F, Vassiliadis P, Menoud P, Beliaeva V, Violante IR, Abderrahmane H, Dzialecka P. Noninvasive theta-burst stimulation of the human striatum enhances striatal activity and motor skill learning. Nat Neurosci 2023:1–12.
[21] Liu A, Vöröslakos M, Kronberg G, Henin S, Krause MR, Huang Y, Opitz A, Mehta A, Pack CC, Krekelberg B, Berényi A, Parra LC, Melloni L, Devinsky O, Buzsáki G. Immediate neurophysiological effects of transcranial electrical stimulation. Nat Commun 2018;9(1):5092. https://doi.org/10.1038/s41467-018-07233-7.
[22] Luff Charlotte E, Peach Robert, Mallas Emma-Jane, Rhodes Edward, Laumann Felix, Boyden Edward S, Sharp David J, Barahona Mauricio, Grossman Nir. The neuron mixer and its impact on human brain dynamics. bioRxiv 2023. https://doi.org/10.1101/2023.01.05.522833. 2023.01.05.522833.
[23] Martinez SC, Goswami C, Forssell M, Cao J, Barth A, Grover P. Cell-specific effects of temporal interference stimulation on cortical function. 2023.
[24] Acerbo E, Jegou A, Luff C, Dzialecka P, Botzanowski B, Missey F, Ngom I, Lagarde S, Bartolomei F, Cassara A, Neufeld E, Jirsa V, Carron R, Grossman N, Williamson A. Focal non-invasive deep-brain stimulation with temporal interference for the suppression of epileptic biomarkers. Front Neurosci 2022;16. https://www.frontiersin.org/articles/10.3389/fnins.2022.945221.
[25] Missey F, Rusina E, Acerbo E, Botzanowski B, Trébuchon A, Bartolomei F, Jirsa V, Carron R, Williamson A. Orientation of temporal interference for non-invasive deep brain stimulation in epilepsy. Front Neurosci 2021;15. https://www.frontiersin.org/articles/10.3389/fnins.2021.633988.
[26] Missey F, Ejneby MS, Ngom I, Donahue MJ, Trajlinek J, Acerbo E, Botzanowski B, Cassarà AM, Neufeld E, Glowacki ED, Shangold L, Hanes WM, Williamson A. Obstructive sleep apnea improves with non-invasive hypoglossal nerve stimulation using temporal interference. Bioelectron Med 2023;9(1):18. https://doi.org/10.1186/s42234-023-00120-7.
[27] Doostdar N, Airey J, Radulescu CI, Melgosa-Ecenarro L, Zabouri N, Pavlidi P, Kopanitsa M, Saito T, Saido T, Barnes SJ. Multi-scale network imaging in a mouse model of amyloidosis. Cell Calcium 2021;95:102365. https://doi.org/10.1016/j.ceca.2021.102365.
[28] Pnevmatikakis EA, Giovannucci A. NoRMCorre: an online algorithm for piecewise rigid motion correction of calcium imaging data. J Neurosci Methods 2017;291:83–94. https://doi.org/10.1016/j.jneumeth.2017.07.031.
[29] de Cheveigné A, Arzounian D. Robust detrending, rereferencing, outlier detection, and inpainting for multichannel data. Neuroimage 2018;172:903–12. https://doi.org/10.1016/j.neuroimage.2018.01.035.
[30] Hines ML, Carnevale NT. The NEURON simulation environment. Neural Comput 1997;9(6):1179–209. https://doi.org/10.1162/neco.1997.9.6.1179.
[31] Hines M, Davison AP, Muller E. NEURON and Python. Front Neuroinf 2009;3:391.
[32] Aberra AS, Peterchev AV, Grill WM. Biophysically realistic neuron models for simulation of cortical stimulation. J Neural Eng 2018;15(6):066023.
[33] Hodgkin AL, Huxley AF. A quantitative description of membrane current and its application to conduction and excitation in nerve. J Physiol 1952;117(4):500.
[34] Berens P. CircStat: a MATLAB toolbox for circular statistics. J Stat Software 2009;31(10):1–21. https://doi.org/10.18637/jss.v031.i10.
[35] Chen T-W, Wardill TJ, Sun Y, Pulver SR, Renninger SL, Baohan A, Schreiter ER, Kerr RA, Orger MB, Jayaraman V, Looger LL, Svoboda K, Kim DS. Ultrasensitive fluorescent proteins for imaging neuronal activity. Nature 2013;499(7458):295–300. https://doi.org/10.1038/nature12354.
[36] Weiss G. Sur la possibilite de rendre comparables entre eux les appareils servant a l'excitation electrique. Arch Ital Biol 1901;35:413.
[37] Lapicque LM. Recherches quantitatives sur l'excitation electrique des nerfs. J Physiol Paris 1907;9:620–35.
[38] Bostock H. The strength-duration relationship for excitation of myelinated nerve: computed dependence on membrane parameters. J Physiol 1983;341(1):59–74.
[39] McIntyre CC, Grill WM. Sensitivity analysis of a model of mammalian neural membrane. Biol Cybern 1998;79:29–37.
[40] McIntyre CC, Grill WM. Extracellular stimulation of central neurons: influence of stimulus waveform and frequency on neuronal output. J Neurophysiol 2002;88(4):1592–604.
[41] Hutcheon B, Yarom Y. Resonance, oscillation and the intrinsic frequency preferences of neurons. Trends Neurosci 2000;23(5):216–22. https://doi.org/10.1016/S0166-2236(00)01547-2.
[42] Ozen S, Sirota A, Belluscio MA, Anastassiou CA, Stark E, Koch C, Buzsáki G. Transcranial electric stimulation entrains cortical neuronal populations in rats. J Neurosci 2010;30(34):11476–85. https://doi.org/10.1523/JNEUROSCI.5252-09.2010.